I&EC research
Industrial & Engineering Chemistry Research

pubs.acs.org/IECR
Article

Ammonia Adsorption by Polyacrylonitrile-Based Carbon Nanofibers

Paula Metschan,* Ansgar Kretzschmar, Hermann Tempel, Eirini Goudeli, Colin A. Scholes, and Rüdiger-A. Eichel

Cite This: *Ind. Eng. Chem. Res.* 2026, 65, 14525−14537

ABSTRACT: Polyacrylonitrile-based carbon nanofibers (PAN-based CNFs) have potential as tunable adsorbents for NH_3 capture from industrial processes, with adsorbent properties controlled by the carbonization temperature. Fibers prepared by electrospinning and carbonized between 800 and 1000 °C were characterized by NH_3 adsorption isotherms at 25 and 50 °C and equilibration curves at 50 and 100 mbar. The NH_3 uptake showed that pore architecture, rather than surface composition, primarily governs both adsorption kinetics and capacity. High affinity toward NH_3 and Type I isotherms were observed for samples carbonized at 800 and 850 °C, associated with specific ultramicropores that provide strong physisorption, as confirmed by the isosteric heat of adsorption. Increasing carbonization temperature reduced pore accessibility, leading to diffusion limitations and lower NH_3 uptake. These findings demonstrate that PAN-based CNFs offer tunable adsorption behavior through control of carbonization temperature and could be used for NH_3 separation and purification at ambient conditions in industrial applications.

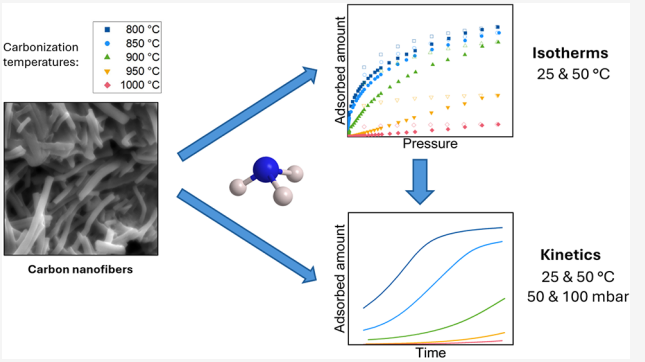

INTRODUCTION

Ammonia (NH_3) is produced in large quantities every year for use in fertilizer production (e.g., urea), refrigerants, explosives, cleaning products and other chemicals.[1] Importantly, NH_3 has significant potential for hydrogen storage, due to its easy liquefaction with minimal energy input, its high volumetric hydrogen density in the liquid state and established regulatory understanding in transport and storage.[2] Industrial NH_3 is primarily generated by the Haber-Bosch process, where hydrogen and nitrogen react over an iron-based catalyst, such as Fe_2O_3 which gets reduced *in situ* to FeO, at very high pressures and temperatures.[3,4] Alternative NH_3 generation methods are focused on near-ambient conditions, mainly utilizing electrochemistry for nitrogen fixation.

The main industrial processes that generate or consume large quantities of NH_3 are summarized in Table 1. These include urea[5] production for fertilizer from CO_2 at moderate temperatures and high pressures, and the manufacture of ammonium nitrate,[6] an explosive formed by neutralizing HNO_3 with NH_3 at moderate temperatures and low to moderate pressures. In the semiconductor industry,[7] NH_3 is also in high demand as a nitrogen source for epitaxial growth, for example in the formation of silicon nitride films by chemical vapor deposition using silane. NH_3 also occurs as an impurity during biogas production[8,9] from nitrogen-rich organic waste.

Even small NH_3 losses in these processes have serious economic implications, and accidental emissions to the atmosphere must be avoided because NH_3 poses significant risks to human health and the environment. Effective NH_3 capture is therefore crucial, but the methods used are often energy intensive or require high maintenance. A very common approach is acid scrubbing, in which NH_3 reacts with an acid to form a salt solution that is subsequently regenerated. However, this process has major drawbacks, including high chemical consumption, an increased risk of corrosion to equipment and exposure of staff to corrosive media as well as operational complexity.[14]

For the subsequent recycling of residual NH_3, other capture methods are necessary where NH_3 remains as a gas so it can be reintroduced to the cycle again. New research into technologies for NH_3 capture from gas streams focuses on solvent absorption by ionic liquids, adsorption by porous solids, ab-adsorption by porous liquids and membrane separation.[15,16] Adsorption by porous solids is an energy-efficient separation technique that can achieve high purity. In an industrial process for the separation of NH_3, such as pressure swing adsorption, the adsorbent material is usually filled into a fixed bed in the form of pellets. Pellets offer several

Received: March 13, 2026
Revised: June 16, 2026
Accepted: June 18, 2026
Published: July 3, 2026

Table 1. Summary of Selected Industrial Synthesis Processes in Which NH_3 Capture Is Relevant

Process	Conditions	NH_3 Concentration (mol %)	Purpose of NH_3
Haber-Bosch Process[3,4,10]	350−500 °C	25−35	Product
$N_2(g) + 3H_2(g) \rightleftharpoons 2NH_3(g)$	150−300 bar		
Electrochemical NH_3 synthesis (e.g., aqueous system)[11]	20−40 °C	5−15	Product
$N_2(g) + 3H_2O(l) \rightarrow 2NH_3(aq) + \frac{3}{2}O_2(g)$	1 bar		
Bosch−Meiser process (Urea)[12]	170−200 °C	40−50	Excess reactant
$2\,NH_3(g) + CO_2(g) \rightleftharpoons CO(NH_2)_2(s) + H_2O(l)$	130−200 bar		
Ammonium nitrate production[6]	100−180 °C	40−50	Excess reactant
$NH_3\,(aq/g) + HNO_3(aq) \rightarrow NH_4NO_3(aq) + heat$	1−10 bar		
Chemical Vapor Deposition e.g., Silicon nitride (Si_3N_4) LPCVD[13]	700−900 °C	80−90	Excess reactant
$3\,SiH_4(g) + 4NH_3(g) \rightarrow Si_3N_4(s) + 12H_2(g)$	0.13−1.3 bar		
Biogas[8,9]	30−60 °C 1 bar	0.05	Impurity

advantages over powders, including a lower pressure drop[17] and higher volumetric capacity through denser packing that allows the use of smaller columns.[18] They are easier to handle and exhibit higher mechanical stability, with little or no dust formation,[19] thereby improving both process efficiency and operational reliability.

For NH_3 adsorption, porous solids include carbonaceous materials, metal−organic frameworks, porous polymers and zeolites.[20] Many of these porous solids exhibit strong adsorption interactions, so significant energy is required to regenerate the material. Others rely on highly specialized production pathways, making their fabrication challenging at scale. Carbon-based materials that have been studied as NH_3 adsorbents include activated carbons, biochar, graphite oxide[21] and activated carbon fibers (ACF).[22] These carbon materials are popular due to their high thermal, mechanical and chemical stability.[23] An optimal adsorbent for NH_3 is chemically stable toward hydrolysis, has a high adsorption capacity, and exhibits a higher affinity for NH_3 than for the other gases present in the mixture. Materials with a high capacity typically possess a large internal surface area, particularly a large micropore volume. This can be evaluated by gas adsorption measurements, and the BET surface area is one common metric for comparing different adsorbent porosities. Affinity can be expressed as heat of adsorption which indirectly reflects the binding strength of NH_3 to the adsorbent. Because of its chemical properties, NH_3 interacts strongly with acidic, oxygen-containing surface functional groups via hydrogen bonds and acid−base interactions. Postoxidation treatment with acids has been shown to increase the number of oxygen-containing groups and thereby enhance the NH_3 binding strength.[24] The process also alters the pore structure, which can increase adsorption capacity. While a high affinity for NH_3 can be beneficial for adsorption selectivity, this comes with an energy penalty, because the bonding energy needs to be overcome during regeneration of the adsorbent. Another way to achieve high affinity of NH_3 to the adsorbent is to tailor the pore structure so that molecules larger than NH_3 are excluded. This separation strategy relies on the molecular sieve effect, in which molecules are separated according to size because only those small enough can diffuse into the pores of the material.[25]

Recently, polyacrylonitrile-based carbon nanofibers (PAN-based CNFs) have emerged as tunable carbon molecular sieves.[26] The ultramicropore and micropore widths in PAN-based CNFs can be finely tuned by selecting a carbonization temperature between 600 and 1100 °C. This unique adaptability enables separation of small gas molecules according to their size and ability to diffuse into ultramicropores. Such size-selective separation has been demonstrated for CO_2 from Ar, N_2 and CH_4 mixtures.[26−28] Critically for this study, PAN-based CNFs have demonstrated the ability to adsorb or exclude NH_3 from their pores at 0 °C, depending on the carbonized temperature.[29]

This study establishes PAN-based CNFs as a distinct class of NH_3 adsorbents in which competitive uptake is achieved predominantly via strong physisorption in ultramicropores, rather than by chemisorption at oxygen-containing surface groups. This physisorption-driven mechanism clearly differentiates PAN-based CNFs from oxidatively modified carbons, MOFs and zeolites, which primarily bind NH_3 through chemisorption at specific active sites and therefore typically suffer from higher regeneration energies. By systematically tuning the carbonization temperature of PAN-based CNFs, the pore morphology and adsorption affinity can be precisely controlled, enabling efficient yet readily regenerable NH_3 capture. NH_3 adsorption isotherms were recorded at 25 and 50 °C, conditions that are directly relevant to industrial operation and comparable to NH_3 recycling processes. In addition, time-resolved equilibration curves at low pressures were obtained on macroscopic pellets exposed to pure NH_3, providing one of the few kinetic data sets for pelletized carbon materials under these conditions and yielding valuable insight into adsorption kinetics and the underlying sorption mechanism. These results demonstrate the potential of PAN-based CNFs as robust, thermally stable and tunable NH_3 adsorbents for industrial applications with low NH_3 concentrations such as electrochemical NH_3 synthesis or biogas upgrading.

MATERIALS AND METHODS

Fabrication of Polyacrylonitrile Carbon Nanofibers

Electrospinning. All chemicals were used as received without further purification. Nanofibers were prepared by electrospinning of a solution containing 6 wt % polyacrylonitrile (PAN) in N,N-dimethylformamide (DMF).

In a typical synthesis, DMF (75.2 g, 99.8%, VWR Chemicals, Germany) was added to PAN (4.8 g, MW = 200,000 g/mol, DOLAN GmbH, Germany). The mixture was stirred for 2 h at 65 °C until a clear solution was obtained. The solution was electrospun in an

https://doi.org/10.1021/acs.iecr.6c01147
Ind. Eng. Chem. Res. 2026, 65, 14525−14537

electrospinning device equipped with a rotating drum collector (Vivolta, formerly IME Medical Electrospinning, The Netherlands) under constant climatic conditions of 25 °C and 30% relative humidity. The PAN/DMF solution was filled into a 20 mL syringe and supplied to the electrospinning device by a syringe pump at 240 μL min^{-1}. A 4-tip spinning needle was used for electrospinning. The needles were moved laterally on an automated spinneret in a range of ±60 mm from the central position with a speed of 20 mm s^{-1} and a turn delay of 500 ms. The acceleration voltage was 26 kV and the distance between needle and collector center was 140 mm. The rotating drum collector had a diameter of 9 cm and was rotating at a speed of 1500 rpm. Electrospinning for 2 h 45 min yielded a colorless, unwoven PAN-nanofiber mat (~14 × 10 cm), which was cut into 3 samples. The samples were then stabilized and cross-linked for 15 h at 250 °C in air using a drying cabinet with an exhaust fan (Binder GmbH, Germany). The heating rate was set to 5 K min^{-1}.

Pellet Production. To produce pellets, the stabilized fibers were ground with a knife mill (IKA A 10 basic, IKA, Germany) with a grinding chamber reduction and a star-shaped cutter for a total of 3 min until a fine powder was obtained. The fibers were mixed with a 6 wt % PAN/DMF solution such that the mass of PAN corresponded to 10 wt % of the fiber mass (PAN:fiber = 1:10 w/w). DMF was added while kneading with a spatula until a homogeneous, dough-like mass was obtained. This mass was extruded through the 2 mm nozzle of a 2 mL syringe onto a Petri-dish into cylindrical lines. These were predried on a heating plate for 2 h at 60 °C and stored overnight in a vacuum drying chamber (Binder, Germany) at 80 °C. The dried extrudate was then broken into 5 mm long pellets with a scalpel.

The stabilized fiber pellets were filled into an alumina crucible which was placed into a horizontal tube furnace (REST-E 400/6, Carbolite Gero GmbH & Co. KG, Germany). Prior to the carbonization, the furnace was evacuated and purged with Ar three times, and the inert gas flow rate was set to 100 l h^{-1}. The sample was heated up to a constant temperature of 800−1000 °C with a heating rate of 5 K min^{-1}. The carbonization temperature was maintained for 3 h. Then, the furnace cooled down at a rate of 200 K h^{-1}. The carbonized samples were stored in a screw lid jar.

MATERIAL CHARACTERIZATION

Surface Characterization

Elemental Analysis. Elemental analysis was conducted on the vario EL cube (Elementar Analysensysteme GmbH, Germany). For the determination of the carbon, hydrogen and nitrogen content, 2 mg of sample were measured in CHN-mode. The oxygen content was determined in O-mode using another 2 mg of sample.

XPS. X-ray photoelectron spectroscopy was used to determine the surface fraction of elements. The measurements were performed on a PHI 5000 VersaProbe II (ULVAC-PHI Inc., USA) with a monochromatic Al K-alpha (1.486 keV) X-ray source. The settings were 50 W, 15 kV and a spot size of 200 μm.

Scanning Electron Microscopy. Scanning electron microscopy investigations were performed using a Quanta FEG 650 microscope (FEI, USA). The images were recorded using an acceleration voltage of 5 kV with a spot size of 2.5 with an Everhart−Thornley detector. The samples were mounted onto the sample holder using double-sided carbon tape.

Gas Adsorption

Porosity Characterization. Isotherms of Ar (Air Liquide, N5.2) and CO_2 (Air Liquide, N4.5) were measured using a 3P micro 300 volumetric sorption analyzer (3P Instruments GmbH & Co. KG, Germany). The samples were degassed under vacuum for at least 4 h at 200 °C prior to measurement. Ar isotherms were recorded at 87 K and CO_2 at 273 K.

Brunauer−Emmett−Teller (BET) areas were determined using ASiQWin software. Isotherm points in the p/p0 range of 0.05−0.3 were chosen. To calculate the pore size distribution for micropores, grand canonical Monte Carlo simulations (GCMC) were applied to the CO_2 isotherms within the ASiQWin software. The simulations utilized a GCMC−CO_2-carbon equilibrium transition kernel at 273 K based on a slit pore model that is applicable to a pore with range between 0.35 and 40 nm. The kernel itself uses a three-center potential function with interactions between the sites of different molecules modeled as a sum of Lennard-Jones and electrostatic contribution.[30]

NH_3 Isotherms. NH_3 adsorption isotherms (Air Liquide, N5.0) have been recorded with an Autosorb iQ instrument (Quantachrome, USA) which was equipped with an external water bath. In a typical experiment at 100−200 mg of a sample were degassed under vacuum for at least 6 h at 200 °C prior to measurement. Static NH_3 isotherms were measured in physisorption mode with a minimum equilibration time of 30 min and a pressure tolerance value of 2 Pa.[31] The measurement of an isotherm under this condition could take between 4 and 7 days.

Isotherm Fits. Isotherms have been modeled in the program OriginLab using custom fit functions according to the empirical Langmuir−Freundlich isotherm model,[32,33]

$$q = \frac{q_m \times (K \times p)^c}{1 + (K \times p)^c} \quad (1)$$

where q is the amount adsorbed (mmol g^{-1}), q_m the maximum amount adsorbed (mmol g^{-1}), p pressure (mbar) and K the affinity constant (mbar^{-1}). The heterogeneity exponent c accounts for distribution in sorption isotherm within the fiber sample, and a value closer to 0 indicates high heterogeneity, while a value of 1 equates to the Langmuir isotherm.[33]

Isosteric Heat of Adsorption. Isosteric heat of adsorption values were calculated using the Clausius−Clapeyron equation.[34]

$$\Delta Q_{st} = R \times \frac{\ln(p_1/p_2)}{\left(\frac{1}{T_1}\right) - \left(\frac{1}{T_2}\right)} \quad (2)$$

Where ΔQ_{st} is the isosteric heat of adsorption and describes the energy change associated with the adsorption process at constant surface coverage, R is the ideal gas constant and T the temperature. From two isotherms at different temperatures, the isosteric heat of adsorption is calculated from points on both isotherms that share the same adsorbed amount. p_1 refers to the equilibrium pressure of the isotherm measured at temperature T_1, which has the same adsorbed amount as the other isotherm at temperature T_2 at an equilibrium pressure p_2.

Equilibration Curves. Equilibration curves of NH_3 were measured using the vector dose mode of Autosorb iQ sorption analyzer (Quantachrome, USA). The equilibration time was set to the maximum value of 99 min and a tolerance value of 0 was selected. In the vector dose mode, a dose amount can be selected for a relative pressure interval. To achieve single point isotherms, only one interval was used with the maximum value being the end point of the equilibration curve. This was either 0.1 or 0.05 bar. The dose amount was calculated from adsorbed amount at set pressure from the full isotherm and

https://doi.org/10.1021/acs.iecr.6c01147
Ind. Eng. Chem. Res. 2026, 65, 14525−14537

depended on the chosen sample mass (between 100 and 200 mg). A detailed description of the calculations can be found in the Supporting Information (S1 to S3).

Kinetics Fits. The equilibration curves were fit to two different kinetics models, the pseudo-first-order kinetics model (PFO):[35]

$$q_t = q_e(1 - \exp(-k_{PFO}t)) \quad (3)$$

and the pseudo-second-order kinetics model (PSO):[36]

$$q_t = \frac{tq_e^2}{\frac{1}{k_{PSO}} + q_e t} \quad (4)$$

In each of these models q_t stands for the adsorbed amount at time t and q_e stands for the adsorbed amount when equilibrium was reached. The parameters k_{PFO} and k_{PSO} represent the kinetic constants of the PFO and the PSO model.

RESULTS AND DISCUSSION

Characterization of PAN-Based CNFs

To confirm the morphology of the PAN-based carbon nanofiber pellets scanning electron microscopy was used. The SEM images of an exemplary pellet carbonized at 1000 °C are provided in Figure 1. The randomly oriented fiber pieces

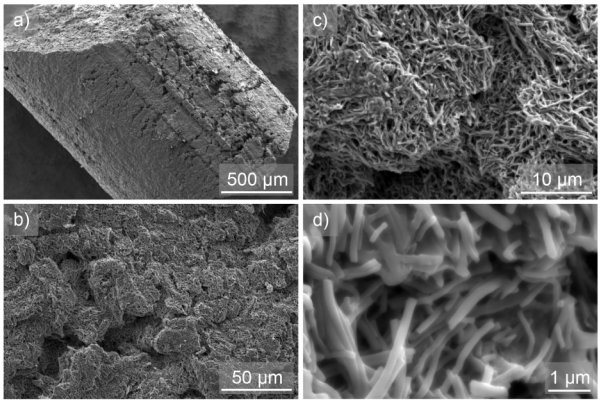

Figure 1. SEM images of a PAN-based CNF pellet carbonized at 1000 °C at different magnifications: (a) 100×, (b) 1000×, (c) 5000×, and (d) 30000×.

are 3−5 µm long and have a diameter of 200−300 nm (Figure 1d). These are comparable to unpelletized PAN-based carbon nanofibers previously reported by the authors.[26] Within the pellet (Figure 1a−c) there are some irregularly shaped macropores (5−50 µm) which allow for gases to diffuse through the carbon structure. Smaller porosity such as micro- or ultramicropores might be present on the fibers, but their dimensions are beyond the resolution of the SEM. Such small pores are usually characterized by gas adsorption methods.

Elemental Analysis and XPS

The chemical functionalities on the surface of the adsorbent also influence its ability to adsorb NH_3, particularly through acid−base interactions with oxygen-containing, acidic, surface functional groups. To determine the chemical composition and potential functional groups on the surface of the carbon nanofibers, two complementary techniques (EA and XPS) were applied. The overall chemical composition for the bulk PAN-based CNF material is provided in Figure 2, based on

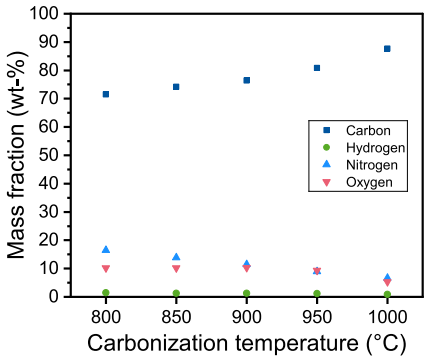

Figure 2. CHNO analysis results for PAN-based CNFs at carbonization temperatures from 800 to 1000 °C. Error bars are not shown because the associated uncertainties (0.04−0.2 wt %) are smaller than the marker size.

CHNO analysis. Across the investigated carbonization temperatures, the fibers consist mainly of carbon, smaller amounts of nitrogen and oxygen, and trace amounts of hydrogen. However, with increasing carbonization temperature from 800 to 1000 °C, the carbon content increases from 70 to 90 wt %, while the nitrogen and oxygen contents decrease correspondingly from 15 to 5 wt % and from 10 to 5 wt %, respectively. Pure PAN has an elemental composition of C:H:N of 3:3:1, with the processing steps after electrospinning responsible for the change in composition, primarily through cyclization, dehydrogenation and oxidation. During the subsequent carbonization, heteroatoms such as oxygen and nitrogen are expelled from the carbon lattice as gases such as HCN, N_2, CO_2.[37] This increases the carbon content and reduces oxygen functionalized groups that may chemisorb NH_3.

The analysis of the oxygen functional groups on the surface of the PAN-based CNF samples was undertaken by XPS, with the outcome provided in Figure 3. The XPS analysis demonstrated low oxygen levels below 5 wt %, indicating that the number of oxygen-containing functional groups is limited and the affinity to NH_3 based on the surface functional groups might be low.

A deconvolution of the oxygen peak shows that it is dominated by single-bonded C−O species, consistent with carboxylic acid, ether or hydroxyl groups. These functionalities can act as hydrogen-bond donors or acceptors and may therefore contribute to attractive interactions with NH_3. In contrast, the fraction of carbonyl-type oxygen, which could correspond to carboxylic acid, carboxylic ester or lactone groups, is very low. This suggests that only a small number of acidic surface sites are present, so strong acid−base interactions with NH_3[38] are expected to be negligible.

The nitrogen-containing surface functionalities consist predominantly of pyridinic and pyrrolic nitrogen species (see SI), which are incorporated into the carbon lattice. These nitrogen sites can form hydrogen bonds[39] with NH_3, but their interaction is expected to be weaker than that of oxygen-containing groups because the C−N bond is less polar than the C−O bond. Taken together, these observations indicate that the interaction energies for NH_3 adsorption lie firmly within the physisorption regime.

Ar Isotherms and BET

For an analysis of the porosity of a material, the evaluation of gas adsorption isotherms of Ar at 87 K is a standard technique.

https://doi.org/10.1021/acs.iecr.6c01147
Ind. Eng. Chem. Res. 2026, 65, 14525−14537

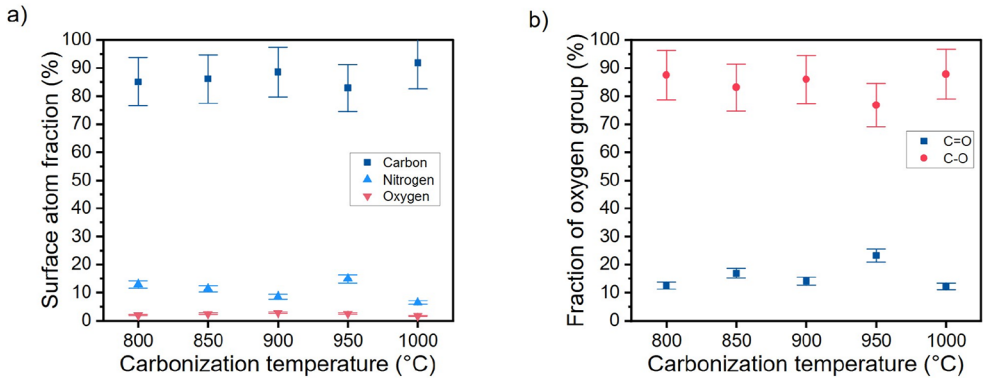

Figure 3. a) Elemental surface composition of PAN-based CNF samples carbonized between 800 and 1000 °C determined by XPS. b) Relative surface fraction of CO-related functionalities obtained from XPS analysis, with error bars indicating the associated uncertainties. The different nitrogen functional groups identified by XPS are shown in the Supporting Information.

The shape of the isotherm provides insights into whether the material is porous. Based on the isotherms, the BET area can be determined, which in this case describes the area covered by a monolayer of Ar at its boiling point. In the literature, a high BET value is typically related to a high adsorption capacity of the material. The Ar isotherms of the PAN-based CNFs and the corresponding BET areas are provided in Figure 4 and Table 2.

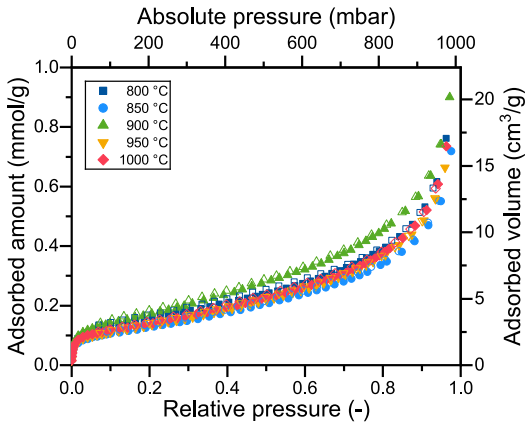

Figure 4. Ar adsorption isotherms measured at 87 K for PAN-based CNFs carbonized between 800 and 1000 °C. Adsorption measurements typically exhibit uncertainties below 5%.

Table 2. BET Surface Areas of PAN-Based CNF Pellets Determined from Ar Adsorption Isotherms at 87 K (see Figure 4)

Carbonization Temperature (°C)	BET Area (m^2 g^{-1})	Correlation Coefficient
800	11.2	0.99996
850	12.6	0.9999
900	9.2	0.9999
950	9.7	0.9998
1000	10.1	0.9998

The Ar isotherms consistently exhibit a Type II shape, which indicates that the adsorbent is nonmicroporous. Additionally, the adsorbed amount shows little variation, suggesting that the surface area is not significantly affected by changes in carbonization temperature. The corresponding BET area is very low and ranges from 9.2 to 12.6 m^2 g^{-1}. The obtained BET areas are in fact very similar to the estimated value of a theoretical nonporous fiber with a diameter of 200 nm (9 m^2 g^{-1}) and marginally lower than PAN-based CNFs from previous works (15 m^2 g^{-1}).[26] The small differences can be attributed to slight variations in preparation conditions, including electrospinning parameters. The low BET areas could generally be an indication that the capacity of NH_3 might be low on this material.

While Ar BET measurements are useful for characterizing mesoporous and macroporous materials, they are not sufficient for accurately describing highly microporous materials with very small pores. This limitation arises because, at 87 K, the diffusion of Ar into ultramicropores is sterically and kinetically hindered. As a result, these very small pores cannot be detected, even if they are present in the material. NH_3 however, has a smaller kinetic diameter (0.26 nm) than Ar and can therefore enter ultramicropores that Ar cannot access. Previous studies on PAN-based CNFs have shown that, in materials carbonized at 800 °C and above, Ar is excluded from the smallest pores.[26]

CO_2 Isotherms

The standard procedure for the characterization of micropores is the adsorption of CO_2 at 273 K.[40] This is because it enables faster diffusion and access to ultranarrow micropores (0.4−1 nm), thus overcoming kinetic limitations of Ar at cryogenic temperatures. The CO_2 isotherms of the PAN-CNF samples carbonized between 800 and 1000 °C are shown in Figure 5a. Depending on the carbonization temperature, the CO_2 isotherms follow one of two trends. The samples carbonized between 800 and 900 °C show a steep increase in their adsorbed amount at low pressures and approach an equilibrium adsorbed amount at higher pressures. This trend is associated with materials that have accessible micropores.[40] The sample carbonized at 900 °C has a slightly lower adsorbed amount at 1 bar (1.8 mmol g^{-1}) compared to 2.2 mmol g^{-1} for 800 and 850 °C. In contrast, the samples carbonized at higher temperatures of 950 and 1000 °C have distinctly different isotherm shapes where the adsorbed amount increases almost linearly over the whole pressure range. Moreover, the adsorption capacity at 1 bar is significantly reduced for the samples carbonized at higher temperatures, with values of 0.3 mmol g^{-1} for the sample carbonized at 950 °C and 0.2 mmol g^{-1} for the sample carbonized at 1000 °C, both clearly lower than for the samples carbonized at lower temperatures. Another difference between the samples is the behavior of

https://doi.org/10.1021/acs.iecr.6c01147
Ind. Eng. Chem. Res. 2026, 65, 14525−14537

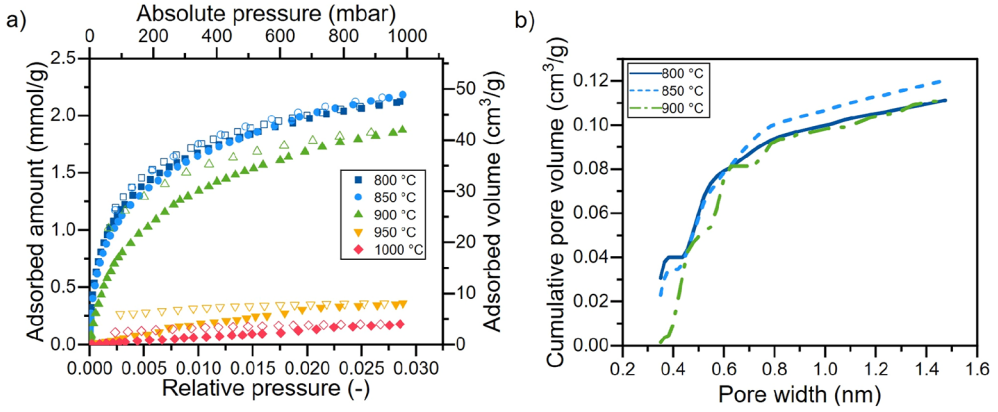

Figure 5. a) CO_2 adsorption isotherms measured at 273 K for PAN-based CNFs carbonized between 800 and 1000 °C. Adsorption measurements typically exhibit uncertainties typically below 5%. b) Cumulative pore volume distribution of the corresponding samples.

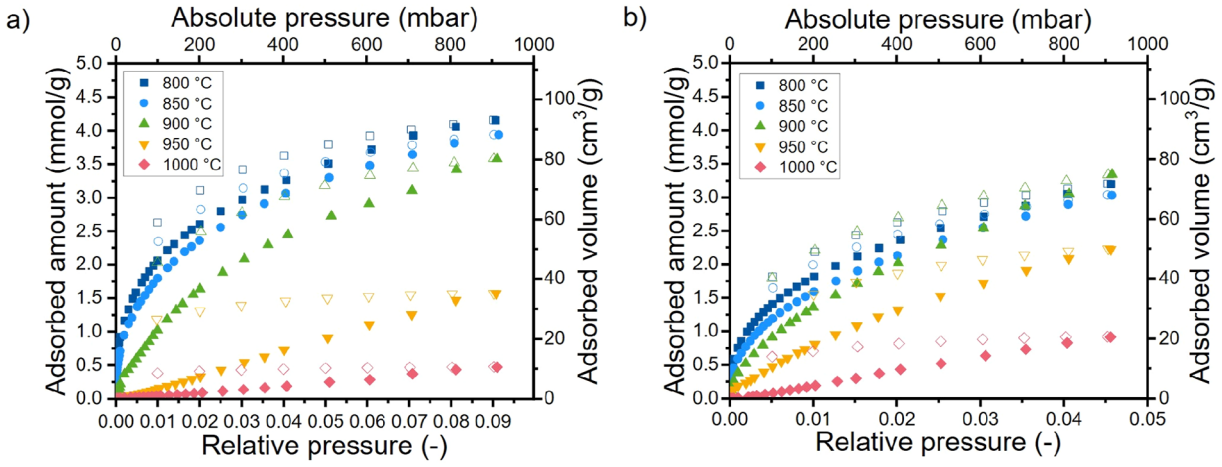

Figure 6. NH_3 adsorption−desorption isotherms on differently carbonized PAN-based CNFs carbonized between 800 and 1000 °C measured at (a) 25 °C and (b) 50 °C, with adsorption data shown as filled symbols and desorption data as open symbols. Adsorption measurements typically exhibit uncertainties typically below 5%.

the desorption curve. Samples that had been carbonized at 800 and 850 °C closely follow the adsorption branch (with a slight difference). This is not the case for the samples carbonized at 900−1000 °C, where the adsorption and desorption branches do not match. This can be attributed to pseudo-irreversibility, arising from slow adsorption and desorption kinetics, which prevent full equilibration within the allotted time.[28] Identical measurement parameters were used for all samples, so differences in pseudo-irreversibility directly reflect kinetic differences.

Pore Size Distribution (Cumulative Pore Volume)

To investigate how the previously described change in adsorption behavior with increasing carbonization temperature can be related to changes in the pore size, Grand Canonical Monte Carlo (GCMC) simulations were performed based on the CO_2 adsorption isotherms to calculate the cumulative pore volume (Figure 5b). Previous investigations on the PAN-based carbon nanofibers have confirmed that these materials possess a turbostratic structure, composed of randomly translated, rotated, or curved carbon layers, parallel to the fiber surface.[41,42] Based on the SAED analysis, it can be inferred that the majority of CO_2 adsorption occurs on the surfaces of these crystallites and within the intercrystallite spaces, which constitute the ultramicroporous network.[42] This structural description is consistent with a pore system that is well represented by slit-shaped pore morphologies. Accordingly, these results support the use of a slit pore model in GCMC simulations for pore-volume characterization of PAN-based CNFs. The pore volume of the ultramicropores was in the range of 0.11 $cm^3\ g^{-1}$. For the samples carbonized at 800 and 850 °C, there are 2 main distributions of pores. The largest pore volume stems from small ultramicropores with a size below 0.4 nm and a second distribution of pores between 0.45 and 0.8 nm. When the carbonization temperature was increased to 900 °C, there were no accessible micropores below 0.4 nm, but larger pores are still present so that the overall pore volume is only slightly smaller. The cumulative pore volume for the samples carbonized at 950 and 1000 °C is not shown because the isotherms are not equilibrated and therefore GCMC simulations would not be physically accurate.

Comparison between Ar and CO_2 Adsorption Isotherms

Ar and CO_2 exhibit markedly different adsorption behaviors on PAN-based CNFs. While Ar isotherms show Type II behavior with negligible pore volume and very low BET surface areas, CO_2 isotherms reveal a significant micropore volume. This discrepancy arises because PAN-based CNFs act as a molecular sieve where the access to the micropores depends on the molecular size of the probe gas. Common ways to

https://doi.org/10.1021/acs.iecr.6c01147
Ind. Eng. Chem. Res. 2026, 65, 14525−14537

describe gas molecule size are for example the kinetic diameter or the critical diameter. Previous studies with various gases have confirmed that only molecules of suitable size can enter these micropores, whereas larger species are sterically excluded. Since Ar is larger than CO_2, it is excluded from the micropores on the PAN-based CNF samples carbonized at 800 °C and above while CO_2 can still access these pores.

The adsorption behavior of CO_2 can be explained by a shrinking pore size with higher carbonization temperatures. While the smallest pores that make up the majority of the pore volume are well accessible to CO_2 on the samples carbonized up to 850 °C, higher carbonization temperatures lead to gradual exclusion from the pores. The higher the carbonization temperature, the smaller the pores get, and the accessibility of CO_2 decreases until it is almost completely excluded from the smallest pores on the sample carbonized at 1000 °C. The onset of the pore exclusion for CO_2 starts at a carbonization temperature of 900 °C, where kinetics get very slow. Likely, most of the smallest pores are in the size range of the CO_2 molecule which makes diffusion into them kinetically restricted. At a carbonization temperature of 950 °C, CO_2 is excluded from the majority of small ultramicropores but a small amount is accessible, which is the reason for the slow kinetics and pseudo-irreversibility.

NH_3 Isotherms

The ability of the PAN-based CNFs carbonized between 800 and 1000 °C to adsorb NH_3 is demonstrated in the isotherms provided in Figure 6, for both 25 and 50 °C.

NH_3 Isotherms at 25 °C

At 25 °C (Figure 6a), there is a clear distinction in the adsorption behavior between PAN-based fibers carbonized at temperatures between 800 and 900 °C, and those carbonized at higher temperatures up to 1000 °C, in keeping with the same behavior observed for CO_2. The isotherms of the samples carbonized at 800 and 850 °C show a Type I behavior with a steep increase in adsorbed amount at low pressures which is associated with micropore filling. At elevated pressures, the adsorbed amount approaches saturation, indicating the progressing occupation of the pore volume. The desorption curves do not closely follow the adsorption curve. The adsorbed amount at 1 bar decreases slightly from 800 to 850 °C from 4.1 mmol g^{-1} to 3.1 mmol g^{-1}. The isotherm of the sample carbonized at 900 °C has a similar overall shape compared to the samples carbonized at lower temperatures. In contrast to the other samples, this isotherm is almost linear at low pressures and becomes curved above ∼100 mbar. Together with the stronger pseudo-irreversibility, this behavior indicates slower sorption kinetics associated with more restricted diffusion into micropores. The isotherms of the samples carbonized at 950 and 1000 °C are practically linear and have a much lower adsorption capacity of NH_3. For the sample carbonized at 1000 °C, a significant fraction of pores is probably smaller than the NH_3 molecule. Both samples show pronounced pseudo-irreversibility, indicating that the isotherms are not equilibrated despite measurement times of up to 7 days. These samples would be expected to adsorb more NH_3 if given sufficient time to reach equilibrium.

This observed pseudo-irreversibility could in principle arise from two effects. First, NH_3 may chemisorb onto surface functional groups, a relatively slow process that could cause apparent hysteresis. If this were dominant, pseudo-irreversibility should decrease with increasing carbonization temperature, as higher temperatures reduce heteroatom content and thus the density of surface functional groups. Moreover, the material generally lacks acidic functional groups on the fibers' surface, so the intermolecular interactions holding NH_3 are too weak to account for significant irreversible binding, which further argues against chemisorption. Hence, the majority of adsorption is expected to occur within the micropores, consistent with Ar measurements showing very limited mesopore and macropore areas. Experimentally, pseudo-irreversibility increases with carbonization temperature, supporting the interpretation that it is predominantly a kinetic effect related to restricted pore accessibility and slower diffusion in progressively smaller pores, rather than a consequence of chemisorption processes. Determining the isosteric heat of adsorption for NH_3 on PAN-based CNFs provides further insight into the nature of the adsorption processes occurring on these materials.

Overall, the fibers carbonized at 800 and 850 °C exhibit good micropore accessibility to NH_3, whereas at 900 °C the micropores are already partially restricted. At carbonization temperatures of 950 °C and above, micropores are still present but become increasingly inaccessible, as indicated by the strong pseudo-irreversibility and lack of equilibrium. This behavior shows that higher carbonization temperatures significantly reduce micropore size, leading to diffusion limitations and restricted NH_3 adsorption on the most highly carbonized samples.

NH_3 Isotherms at 50 °C

The isotherms measured at 50 °C (Figure 6b) have broadly similar shapes to those at 25 °C but show several notable differences: for the samples carbonized at 800 and 850 °C, the adsorbed amount is slightly lower at a relative pressure of 0.04 compared to the measurement at 25 °C. This effect is caused by increased kinetic motion at higher temperatures.

A marked change is observed for the sample carbonized at 900 °C. At 50 °C, it clearly follows a curved shape indicating that the accessibility of the micropores has increased. This may be attributed to thermal expansion of the fibers and opening of the micropores enough to enable NH_3 sorption or to higher kinetic energy that allows for faster diffusion into the pores. Additionally, the adsorbed amount is now higher as well and very similar to that of the samples carbonized at 800 and 850 °C also measured at 50 °C.

The isotherm of the sample carbonized at 950 °C now shows a higher adsorption capacity compared to the measurement at 25 °C as well. Moreover, it now clearly follows a curved shape, and the pseudo-irreversibility is smaller as well, indicating a higher degree of equilibration. This demonstrates that NH_3 can access micropores that are present within the fibers, due to the higher kinetic energy at higher temperature. This indicates that NH_3 is not completely excluded at 950 °C. Rather, diffusion kinetics are very slow at 25 °C.

At 50 °C, the isotherm of the sample carbonized at 1000 °C is still linear and reaches a higher adsorbed amount compared to the measurement at 25 °C but pseudo-irreversibility is still present. The increase in adsorption capacity with temperature suggests that additional micropore volume becomes accessible, but diffusion is still very slow due to the small pore size.

Comparison Between CO_2 and NH_3

Overall, both CO_2 and NH_3 exhibit a similar size-exclusion threshold, with clear molecular sieve behavior emerging for samples carbonized at and above 900 °C. At the same relative

https://doi.org/10.1021/acs.iecr.6c01147
Ind. Eng. Chem. Res. 2026, 65, 14525−14537

pressure, NH_3 consistently shows a higher uptake than CO_2 for all samples, even though the measurements were performed at different temperatures. CO_2 adsorption at higher temperatures would be expected to yield slightly lower uptake, so this comparison remains qualitative. The higher NH_3 uptake can be rationalized by the fact that the molar volume of CO_2 in the adsorbed phase, which is theoretically treated as a liquid-like phase, is roughly twice that of NH_3. Consequently, the available pore volume is filled by fewer CO_2 molecules than NH_3 molecules, leading to an apparently lower uptake for CO_2 at comparable relative pressures. Sorption kinetics are markedly slower for NH_3 than for CO_2, as evidenced by the more pronounced pseudo-irreversibility despite longer equilibration times.

This kinetic difference is plausibly due to their distinct chemical interactions with the PAN-based CNF surface: CO_2, as a Lewis acid, can form favorable interactions with basic, nitrogen-containing surface groups, whereas NH_3, being a Lewis base, does not interact as favorably with these nitrogen sites, and the relatively low content of oxygen functionalities cannot fully offset this potential repulsion, leading to comparatively slower NH_3 adsorption overall. It is also possible that, on specific high-affinity sites, NH_3 interacts more strongly with the surface than CO_2. This is suggested by the steeper initial slope of the NH_3 adsorption isotherm at comparable partial pressures, which indicates a higher affinity on these sites. Such stronger, more specific interactions may involve an activation energy, so that although the equilibrium affinity is higher, the approach to equilibrium is slower, further contributing to the observed kinetic differences between NH_3 and CO_2.

■ ISOSTERIC HEAT OF ADSORPTION

For an understanding of the affinity and binding strength of NH_3 to the PAN-based CNFs, the isosteric heat of adsorption has been calculated using the Clausius−Clapeyron method. In this method, adsorption isotherms of the same material at a minimum of three temperatures are required. First, the isotherm data were fitted to an isotherm model to interpolate between data points. The isotherms of the sample carbonized at 800 °C, measured at 25, 30, 35 and at 50 °C, were fitted to the Langmuir−Freundlich model, which describes multilayer adsorption on a heterogeneous surface with a distribution of adsorption sites with different adsorption enthalpies. A demonstration of the quality of the fits are provided in Figure 7, and the resulting parameters are given in Table 3.

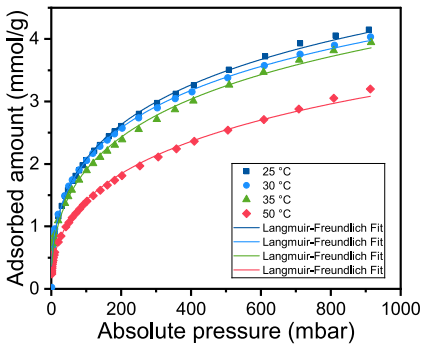

Figure 7. NH_3 adsorption isotherms of the sample carbonized at 800 °C, measured at 25, 30, 35, and 50 °C, together with their Langmuir−Freundlich fits.

Table 3. Fit Parameters of the Langmuir−Freundlich Isotherm Model for NH_3 Adsorption on PAN-Based CNFs Carbonized at 800 °C, Obtained from the Isotherms Measured at 25, 30, 35, and 50 °C (shown in Figure 7)

Temperature (°C)	q_m (mmol g^{-1})	K (10^{-4} $mbar^{-1}$)	c (−)	R^2
25	10	4.9	0.44	0.99889
30	9.8	4.5	0.43	0.99467
35	9.6	4.5	0.45	0.99727
50	9	2.7	0.46	0.99760

The Langmuir−Freundlich fits yielded saturation capacities, q_m, in the range of 9−10 mmol g^{-1}. The fits for the isotherms from 25 to 50 °C show a small, gradual reduction in q_m from 10 to 9 mmol g^{-1}, as adsorption becomes less favorable with increasing temperature. This is also reflected in the value of the affinity constant K, which decreases slightly with increasing temperature. The heterogeneity constant c remains almost identical, indicating little surface change with temperature, as expected, since the same material was used.

From these isotherm fits, the isosteric heat of adsorption was calculated as shown in Figure 8. The isosteric heat of

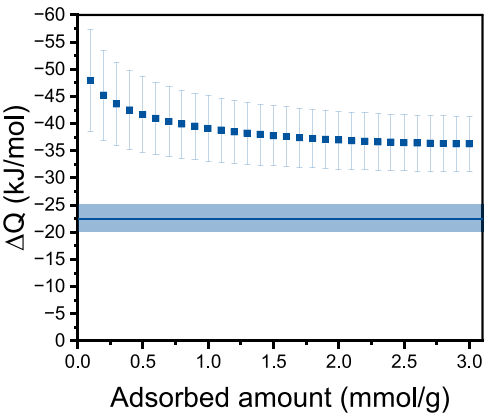

Figure 8. Isosteric heat of NH_3 adsorption for PAN-based CNFs carbonized at 800 °C, calculated using Langmuir−Freundlich fits. Error bars indicate the uncertainty of the calculation. For comparison, the enthalpy of condensation of NH_3 is shown as a reference line.

adsorption is especially high at low adsorbed amounts and decreases slightly at higher adsorbed amounts. Between 0.1 and 1 mmol g^{-1} it reaches an average value of −42 ± 3 kJ mol^{-1} whereas at higher loadings (1.1 to 3 mmol g^{-1}) it decreases to −37 ± 1 kJ mol^{-1}. This behavior is typical for microporous materials and arises because energetically favorable ultramicropores are filled first owing to the confinement effect of overlapping pore-wall potentials.[43] Once the smallest pores were filled, progressively lower-energy sites are occupied, which are associated with a lower heat of adsorption. The error at low adsorbed amounts is three times as high as at higher adsorbed amounts. We therefore focus on the second value of −37 ± 1 kJ mol^{-1} for the isosteric heat of adsorption. This lies in the upper range of physisorption, meaning that NH_3 has a high affinity for the material, but remains reversibly bound to the pores and surface.

The isosteric heat for the PAN-based CNFs is similar to that of viscose-based ACFs (−36 kJ mol^{-1}).[24] This indicates that the observed process is predominantly physisorption with moderate binding strength. However, the PAN-based CNF material has a much lower oxygen content than the viscose-

https://doi.org/10.1021/acs.iecr.6c01147
Ind. Eng. Chem. Res. 2026, 65, 14525−14537

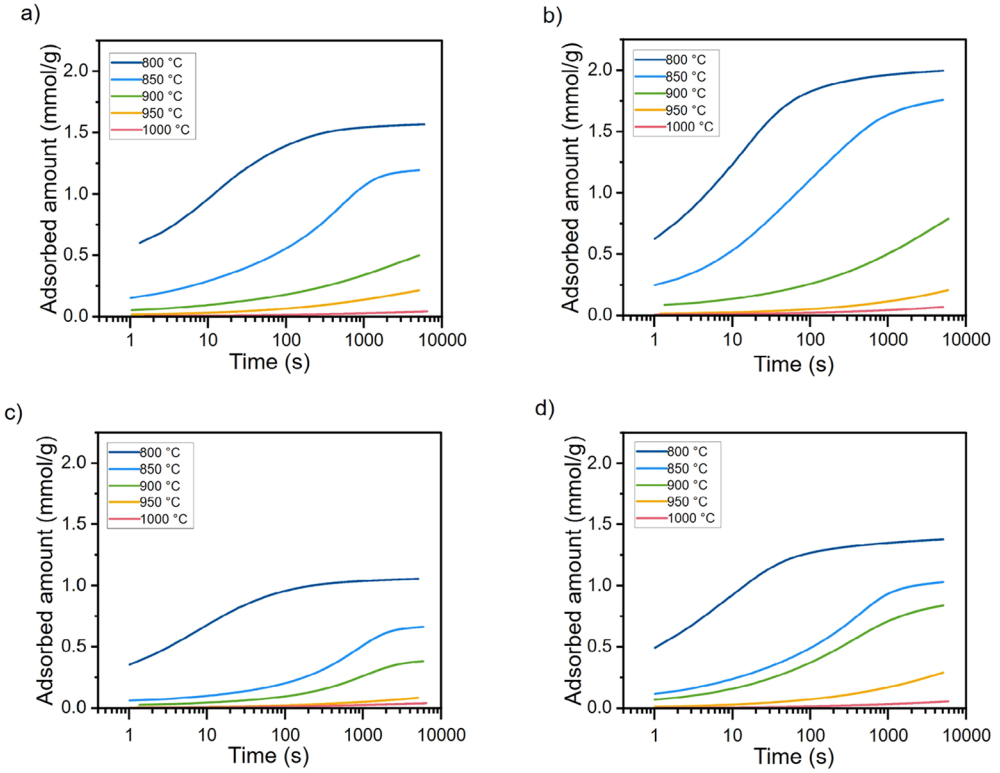

Figure 9. Equilibration curves of NH_3 on differently carbonized PAN-based CNFs (carbonization temperatures are indicated in the legend) at different temperatures and pressures: a) 25 °C and 50 mbar, b) 25 °C and 100 mbar, c) 50 °C and 50 mbar, and d) 50 °C and 100 mbar. Time is plotted on a logarithmic scale to better illustrate the saturation behavior over extended periods. Adsorption measurements in this pressure range typically exhibit uncertainties typically below 5%.

based ACFs, suggesting that the high value comes from a different mechanism. It is likely due to adsorption in ultramicropores, which can be quite strong. For the calculation of isosteric heats of adsorption, only the sample carbonized at 800 °C has been considered, because the Langmuir–Freundlich model is valid only for equilibrated isotherms. Since the sample with the lowest carbonization temperature has the highest pore accessibility, it also shows the lowest pseudo-irreversibility and should therefore be described most accurately by the model. Considering the loss of heteroatoms with increasing carbonization temperature, the heat of adsorption may be slightly lower for the samples carbonized at higher temperatures.

NH_3 Adsorption Kinetics

The kinetics of NH_3 adsorption have been measured at two different equilibrium pressures (50 and 100 mbar) and two temperatures (25 and 50 °C), as shown in Figure 9.

At 50 mbar and 25 °C, the PAN-based CNFs carbonized at 800 °C reached equilibrium within the 2 h measurement time, while the 850 °C sample also equilibrated, albeit over a slightly longer period. In contrast, the samples carbonized at 900, 950, and 1000 °C remained far from equilibrium within the experimental time window. When the measurement temperature was increased to 50 °C, a significant change was observed for the sample carbonized at 900 °C, which then reached equilibrium, whereas the more highly carbonized samples (950 and 1000 °C) were still clearly far from equilibrium. The equilibration measurements at 100 mbar showed essentially the same behavior for all samples, including the same temperature-dependence of equilibration, indicating no qualitative dependence on pressure under the conditions studied. Fully equilibrated measurements could not be obtained for the samples carbonized at 950 and 1000 °C within the maximum equilibration time allowed by the software. Achieving equilibrium would probably require durations of several days.

The strong slowing of the adsorption kinetics at higher carbonization temperatures implies that the micropores become increasingly restricted in size, which hampers the diffusion and adsorption of NH_3. For separation processes, the slow kinetics of these highly carbonized fibers would require residence times that are impractically long for industrial NH_3 removal. Consequently, not only was it experimentally impossible to obtain fully equilibrated measurements within reasonable times for these samples, but they are also not suitable for applications relying on specific and efficient NH_3 adsorption.

Modeling

The equilibration curves were modeled using the pseudo-first-order (PFO) and pseudo-second-order (PSO) kinetic models to gain insight into the adsorption mechanism. In the PFO model, the adsorption rate depends only on the concentration of the adsorbate and is diffusion controlled. Therefore, it works well for physisorption processes, which are rather weak and depend mainly on the nature of the adsorbate. In this case, the number of adsorption sites is effectively unlimited, as adsorption can occur anywhere on the surface, including in multilayers. The PSO model, by contrast, describes processes that are dependent on both the concentration of adsorbate molecules and the number of "active sites" on the adsorbent. This model is often associated with the specific and stronger chemisorption processes.[44−46]

https://doi.org/10.1021/acs.iecr.6c01147
Ind. Eng. Chem. Res. 2026, 65, 14525−14537

The adsorption equilibration data of NH_3 on the samples carbonized at 800−900 °C could be described satisfactorily by the PSO model. For some experimental conditions, the data could not be fitted, owing to the complexity of the microporous structure of the materials. The resulting fit parameters are summarized in Table 4 and shown in Figure 10.

Table 4. Fit Parameters of the PSO Model[a]

Conditions	Carbonization Temperature (°C)	q_e (mmol g^{-1})	k_{PSO} (g $mmol^{-1}$ s^{-1})	R^2
25 °C 50 mbar	800	1.57	0.0624	0.9355
	850	1.237	0.00506	0.97
	900	0.516	0.00434	0.925
25 °C 100 mbar	800	2	0.059	0.925
	850	1.78	0.00773	0.958
	900	0.95	0.00101	0.854
50 °C 50 mbar	800	1.055	0.1134	0.915
	850	0.7	0.0042	0.982
	900	0.42	0.00424	0.99
50 °C 100 mbar	800	1.38	0.099	0.82
	850	1.06	0.00676	0.9778
	900	0.87	0.00562	0.854

[a]The equilibrium uptake q_e was kept fixed, and only the rate constant k_{PSO} was fitted.

The equilibrium adsorbed amount, q_e, decreased for all samples when the temperature was raised from 25 to 50 °C (Figure 10a), which is consistent with the thermodynamic shift of the adsorption−desorption equilibrium toward desorption at higher temperature.

For the sample carbonized at 800 °C, the adsorption rate constant k_{PSO} was slightly higher at 50 mbar than at 100 mbar; however, within experimental uncertainty, k_{PSO} was essentially independent of pressure and showed a clear increase with temperature. This trend is expected, as higher temperatures provide additional thermal energy that facilitates diffusion into the pores and thus accelerates sorption. For the samples carbonized at 850 and 900 °C, the adsorption rate constants (Figure 10b) were of the same order of magnitude and appeared largely independent of temperature and pressure within the investigated ranges.

The fact that the equilibrated adsorption data were well described by the PSO model at 50 and 100 mbar and at 25 and 50 °C indicates that diffusion into ultramicropores is the dominant mechanism and the rate-controlling step of the adsorption process under these conditions.

Diffusion-Limited Physisorption Mechanism

Although the pseudo-second-order kinetic model is often associated with chemisorption, several observations indicate that uptake of ammonia on PAN based carbon nanofibers proceeds via physisorption. Chemisorption would require strong bonding to specific surface functional groups, yet elemental analysis and XPS show only aromatic nitrogen, which can at most engage in hydrogen bonding, and a very small amount of oxygen that cannot be clearly assigned to reactive sites. The isosteric heat of adsorption of −37 to −42 kJ mol^{-1} also lies in the typical range for physisorption. Adsorption kinetics are generally slow and become even slower with increasing carbonization temperature, which confirms that the observed pseudo-irreversibility arises from insufficient equilibration rather than from chemisorption. Pore size analysis with GCMC based on CO_2 adsorption reveals decreasing pore accessibility with increasing carbonization temperature, most likely due to pore shrinkage, and even sub-Ångström changes in micropore diameter can have a strong impact on diffusion and adsorption rates.[47] These findings indicate a diffusion-limited physisorption mechanism governed by micropore accessibility rather than surface chemistry.

Comparison of Adsorption Properties and Their Underlying Chemical Origins

The key physicochemical and adsorption properties of the PAN-based CNFs are benchmarked against a range of literature-reported carbon materials in Table 5. This comparison highlights their adsorption performance in terms of capacity and kinetics under low-pressure NH_3 conditions.

PAN-based carbon nanofibers (PAN-based CNFs) differ markedly from other carbonaceous NH_3 adsorbents in how they balance adsorption capacity, isosteric heat of adsorption, and the relative roles of physisorption and chemisorption, especially at low pressures.

At 25 °C and 100 mbar, PAN-based CNFs reach an NH_3 uptake of 2.2 mmol g^{-1}, about twice that of commercial activated carbon Type A[48] (1.0 mmol g^{-1}) but lower than viscose-based activated carbon nanofibers (5 mmol g^{-1}). At 1 bar, the PAN-based CNF sample carbonized at 800 °C shows the lowest capacity among the materials considered, reflecting its more limited overall porosity compared with highly optimized activated carbons and oxidized carbon fibers.

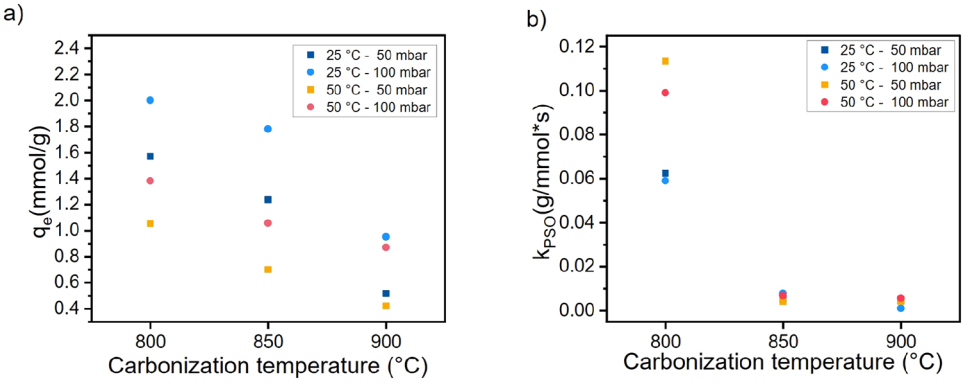

Figure 10. a) Equilibrium adsorbed amount q_e and b) kinetic constant k_{PSO} obtained from pseudo-second-order fits to the equilibration curves for samples carbonized between 800 and 900 °C. No error bars are shown in (a) because q_e was fixed during fitting, and in (b) because the uncertainties (between 7×10^{-6} and 8.5×10^{-4} g $mmol^{-1}$ s^{-1}) are smaller than the symbol size.

https://doi.org/10.1021/acs.iecr.6c01147
Ind. Eng. Chem. Res. 2026, 65, 14525−14537

Table 5. Properties of PAN-Based CNFs Compared with Literature-Reported Carbon Materials[a]

Material	Mechanism of Adsorption	Low Pressure Adsorption Capacity (mmol g^{-1})	Isosteric Heat of Adsorption (kJ mol^{-1})	Kinetics Constants			Source
				Method	Model	Rate Constant	
PAN-based CNF pellets 800 °C	Physisorption in narrow ultramicropores	2 (100 mbar)	37−42	SEQ	PSO	0.0624 g $mmol^{-1}$ s^{-1}	This work
Viscose-based ACF	Physisorption in ultramicropores and chemisorption to oxygen groups	5 (100 mbar)	36.6	-	-	-	Niu et al. 2023[24]
Viscose-based ACF-O	Physisorption in ultramicropores and chemisorption to oxygen groups	6 (100 mbar)	65	DCB	Yoon−Nelson	0.18 1 min^{-1}	Yin et al. 2025[22]
Activated carbon Type A	Physisorption	1 (100 mbar)	26	-	-	-	Cardenas et al. 2023[48]
Commercial activated carbon (B. GmbH 2016)	-	0.47 (500 ppm of NH_3, 40% RH, 20% O_2)	-	-	-	-	Hindocha et al. 2017[49]

[a]Rate constants are only comparable where the experimental method and kinetic model are identical. DCB: dynamic column breakthrough; SEC: static equilibration curve.

The isosteric heat of adsorption further highlights the distinctive adsorption mechanism of PAN-based CNFs. Activated carbon Type A[48] exhibits a relatively low isosteric heat (about 26 kJ mol^{-1}), consistent with weak physisorption on a largely nonfunctionalized carbon surface. Oxidized activated carbon fibers (ACF-O),[22] in contrast, show a much higher isosteric heat (about 65 kJ mol^{-1}), indicating a strong contribution from chemisorption at abundant oxygen-containing sites in addition to physisorption in narrow pores. Viscose-based activated carbon nanofibers[24] lie between these extremes, with an intermediate isosteric heat (about 36.6 kJ mol^{-1}) arising from a combination of physisorption in fine pores and chemisorption at a moderate density of oxygen functional groups.

PAN-based CNFs have a relatively low oxygen content, so they offer fewer chemisorption sites for NH_3 than the oxidized and viscose-based carbons. Nevertheless, their isosteric heat of adsorption is moderate to high (about −37 to −42 kJ mol^{-1}), which is notable given the scarcity of surface oxygen-containing groups. This indicates that NH_3 is stabilized predominantly by strong physisorption within very narrow (ultramicroporous) regions rather than by extensive chemisorption. As a result, PAN-based CNFs show limited total capacity at higher pressures but comparatively strong affinity and enhanced performance at low pressure, where strong confinement in ultramicropores can partially compensate for the lower density of chemisorption sites.

Regarding adsorption kinetics, among the comparable carbon materials considered, only ACF-O has a reported kinetic constant for NH_3 uptake. However, this was extracted from dynamic breakthrough experiments using the Yoon−Nelson model, whereas the kinetic analysis for PAN-based CNFs in this work is based on the pseudo-second-order (PSO) model. Because these models rely on different assumptions and fitting strategies, the resulting rate constants are not directly comparable, and any apparent differences in kinetics between ACF-O and PAN-based CNFs must be interpreted with caution.

Application of PAN-Based CNFs as an Adsorbent for NH_3 Capture from Industrial Processes

PAN-based carbon nanofibers carbonized at 800 °C exhibit relatively high low-pressure adsorption capacity, making them suitable for capturing trace NH_3 concentrations. At this carbonization temperature, they also show somewhat faster adsorption kinetics than materials treated at higher temperatures, enabling rapid uptake and release cycles. In addition, their moderate heat of adsorption provides a reasonable balance between NH_3 affinity and energy efficiency: interactions with adsorbed species are strong enough to ensure good adsorption preference for NH_3, yet weak enough that regeneration can be achieved with relatively low energy input. These properties make the material a viable option for capturing NH_3 from industrial gas streams that contain low NH_3 concentrations, such as those encountered in green ammonia production by electrolysis or in biogas upgrading.

CONCLUSION

In this work, the adsorption properties of polyacrylonitrile-based carbon nanofibers (PAN-based CNFs) toward NH_3 were systematically investigated by varying the carbonization temperature between 800 and 1000 °C and measuring adsorption isotherms at 25 and 50 °C, including kinetic analysis at 0.05 and 0.1 bar. PAN-based CNFs were shown to successfully adsorb NH_3, with the highest uptake achieved for fibers carbonized at 800−900 °C, where a predominantly microporous structure produced Type I isotherms characteristic of micropore filling and strong yet reversible physisorption (isosteric heat of adsorption ∼−37 kJ mol^{-1}). The adsorption rate increased with temperature but was largely independent of pressure. For the sample that was carbonized at 800 °C the kinetics were well described by a pseudo-second-order model, and the rate constant increased by roughly an order of magnitude for measurements at temperatures at 25 and 50 °C. In contrast, samples carbonized at 950−1000 °C exhibited significantly reduced NH_3 uptake, attributed to very slow diffusion into less accessible ultramicropores, consistent with a physisorption mechanism governed by size exclusion. This trend is corroborated by CO_2 isotherms that similarly reflected changes in ultramicropore accessibility. Overall, these results demonstrate that the pore structure of PAN-based CNFs can be finely tuned via carbonization temperature to balance accessibility and selectivity, yielding ultramicroporous adsorbents with high affinity and size-selective uptake of pure NH_3 at low partial pressures. This combination of strong physisorption, controllable pore architecture and molecular-sieving capability suggests that PAN-based CNFs offer distinct

https://doi.org/10.1021/acs.iecr.6c01147
Ind. Eng. Chem. Res. 2026, 65, 14525−14537

advantages over many conventional carbon adsorbents that rely primarily on high surface oxygen content or broad pore size distributions, and identifies them as candidates for NH_3 separation and purification from dilute gas mixtures under near-ambient process conditions, which should be explored in future studies.

■ ASSOCIATED CONTENT

Data Availability Statement

The data underlying this study will be available under a CC BY 4.0 license in Jülich DATA at [10.26165/JUELICH-DATA/S2XWPM] following the publication of this paper.

Supporting Information

The Supporting Information is available free of charge at https://pubs.acs.org/doi/10.1021/acs.iecr.6c01147.

Information on calculations for the measurement of equilibration curves, XPS spectra, NH_3 adsorption isotherms for the calculation of isosteric heat of adsorption, equilibration curve fits, comparison of NH_3 adsorption isotherms for pellets and fibers at 25 °C, and comparison of literature materials with PAN-based CNFs (PDF)

■ AUTHOR INFORMATION

Corresponding Author

Paula Metschan − *IET-1, Forschungszentrum Jülich GmbH, Jülich 52428, Germany; IPC, RWTH Aachen University, Aachen 52057, Germany; Department of Chemical Engineering, The University of Melbourne, Parkville, Victoria 3010, Australia;* orcid.org/0009-0004-8107-7559; Email: p.metschan@fz-juelich.de

Authors

Ansgar Kretzschmar − *IET-1, Forschungszentrum Jülich GmbH, Jülich 52428, Germany*

Hermann Tempel − *IET-1, Forschungszentrum Jülich GmbH, Jülich 52428, Germany;* orcid.org/0000-0002-9794-6403

Eirini Goudeli − *Department of Chemical Engineering, The University of Melbourne, Parkville, Victoria 3010, Australia*

Colin A. Scholes − *Department of Chemical Engineering, The University of Melbourne, Parkville, Victoria 3010, Australia;* orcid.org/0000-0002-3810-2251

Rüdiger-A. Eichel − *IET-1, Forschungszentrum Jülich GmbH, Jülich 52428, Germany; IPC, RWTH Aachen University, Aachen 52057, Germany; Faculty of Mechanical Engineering, RWTH Aachen University, Aachen 52056, Germany;* orcid.org/0000-0002-0013-6325

Complete contact information is available at: https://pubs.acs.org/10.1021/acs.iecr.6c01147

Author Contributions

P.M.: Writing—original draft, Visualization, Methodology, Investigation, Conceptualization. A.K.: Writing—review and editing, Supervision, Methodology, Conceptualization. E.G.: Writing—review and editing, Supervision. C.S.: Writing—review and editing, Supervision, Conceptualization. H.T.: Writing—review and editing, Supervision, Project administration, Funding acquisition. R.-A.E.: Supervision, Project administration, Funding acquisition, Conceptualization.

Notes

The authors declare no competing financial interest.

■ ACKNOWLEDGMENTS

The authors acknowledge funding provided by the Deutsche Forschungsgemeinschaft (DFG, German Research Foundation) under Germany's Excellence Strategy-Cluster of Excellence 2186 'The Fuel Science Center' ID: 390919832 and by Forschungszentrum Jülich GmbH under the program JUMPA.

■ REFERENCES

(1) Aziz, M.; Wijayanta, A. T.; Nandiyanto, A. B. D. Ammonia as Effective Hydrogen Storage: A Review on Production, Storage and Utilization. *Energies* **2020**, *13* (12), 3062.

(2) Jiao, F.; Xu, B. Electrochemical Ammonia Synthesis and Ammonia Fuel Cells. *Adv. Mater.* **2019**, *31* (31), 1805173.

(3) Giddey, S.; Badwal, S. P. S.; Kulkarni, A. Review of Electrochemical Ammonia Production Technologies and Materials. *Int. J. Hydrogen Energy* **2013**, *38* (34), 14576−14594.

(4) Erfani, N.; Baharudin, L.; Watson, M. Recent Advances and Intensifications in Haber-Bosch Ammonia Synthesis Process. *Chem. Eng. Process* **2024**, *204*, 109962.

(5) Masjedi, S. K.; Kazemi, A.; Moeinnadini, M.; Khaki, E.; Olsen, S. I. Urea Production: An Absolute Environmental Sustainability Assessment. *Sci. Total Environ.* **2024**, *908*, 168225.

(6) Zapp, K.-H.; Wostbrock, K.-H.; Schäfer, M.; Sato, K.; Seiter, H.; Zwick, W.; Creutziger, R.; Leiter, H. Ammonium Compounds. In *Ullmann's Encyclopedia of Industrial Chemistry*; John Wiley & Sons, Ltd, 2000. DOI: .

(7) Chen, F.-Y.; Yeh, M.-P.; Lee, S. L.; Chen, T.; Chuang, T.-S.; Tseng, H.-H.; Tung, K.-L. Inorganic Acid and Ammonia Emission Factors in Semiconductor Processes. *Sci. Total Environ.* **2025**, *999*, 180339.

(8) Deublein, D.; Steinhauser, A. *Biogas from Waste and Renewable Resources: An Introduction*; 3rd ed.; Wiley-VCH: Weinheim, 2008.

(9) Weiland, P. Biogas Production: Current State and Perspectives. *Appl. Microbiol. Biotechnol.* **2010**, *85* (4), 849−860.

(10) Appl, M. Ammonia 2. Production Processes. In *Ullmann's Encyclopedia of Industrial Chemistry*; John Wiley & Sons, Ltd, 2011. DOI: .

(11) Allen, J.; Panquet, S.; Bastiani, A. Electrochemical Ammonia: Power to Ammonia Ratio and Balance of Plant Requirements for Two Different Electrolysis Approaches. *Front. Chem. Eng.* **2021**, *3*, 765457.

(12) Meessen, J. H. Urea. In *Ullmann's Encyclopedia of Industrial Chemistry*; John Wiley & Sons, Ltd, 2010. DOI: .

(13) Wang, L.; Xie, W.; Van Thourhout, D.; Zhang, Y.; Yu, H.; Wang, S. Nonlinear Silicon Nitride Waveguides Based on a PECVD Deposition Platform. *Opt. Express* **2018**, *26* (8), 9645.

(14) Ashtari, A. K.; Majd, A. M. S.; Riskowski, G. L.; Mukhtar, S.; Zhao, L. Removing Ammonia from Air with a Constant pH, Slightly Acidic Water Spray Wet Scrubber Using Recycled Scrubbing Solution. *Front. Environ. Sci. Eng.* **2016**, *10* (6), 3.

(15) Jiang, H.-Y.; Wang, Z.-M.; Sun, X.-Q.; Zeng, S.-J.; Guo, Y.-Y.; Bai, L.; Yao, M.-S.; Zhang, X.-P. Advanced Materials for NH_3 Capture: Interaction Sites and Transport Pathways. *Nano Micro Lett.* **2024**, *16* (1), 228.

(16) Akhand, A.; Wu, X.-Y. Current Research on Gaseous Ammonia Detecting and Capture Technologies. *Curr. Opin Environ. Sci. Health* **2023**, *36*, 100515.

(17) Nguyen, X. C.; Kang, J.-H.; Bang, G.; Kim, K.-M.; Lee, C.-H. Pelletized Activated Carbon-Based CO-Selective Adsorbent with Highly Oxidation-Stable and Aggregation-Resistant Cu(I) Sites. *Chem. Eng. J.* **2023**, *451*, 138758.

(18) Marcinek, A.; Guderian, J. Process-Based Evaluation of Adsorbents: Effect of CMS Pellet Size on N_2-PSA Performance. *Adsorption* **2023**, *29* (7), 363−375.

(19) Temmerman, M.; Rabier, F.; Jensen, P. D.; Hartmann, H.; Böhm, T. Comparative Study of Durability Test Methods for Pellets and Briquettes. *Biomass Bioenergy* **2006**, *30* (11), 964−972.
(20) Yao, W.; Wu, W.; Liu, Y.; Zhu, B.; Xiao, J.; Zhang, T.; Xi, S. The Development Prospects and Potential of High Specific Surface Area Materials: A Review of the Use of Porous Framework Materials for the Capture and Filtration of Ammonia. *Molecules* **2025**, *30* (8), 1737.
(21) Bandosz, T. J. Towards Understanding Reactive Adsorption of Small Molecule Toxic Gases on Carbonaceous Materials. *Catal. Today* **2012**, *186* (1), 20−28.
(22) Yin, H.; Zhang, W.; Lu, Y.; He, Z.; Miao, G.; Yang, C.; Xiao, J. Fast and High-Capacity Capture of Trace Ammonia in Confined Space over Oxygen-Rich Activated Carbon Fiber Felt. *Sep. Purif. Technol.* **2025**, *360*, 130915.
(23) Yang, R. T. *Gas Separation By Adsorption Processes*; World Scientific, 1997.
(24) Niu, Y.; Zheng, C.; Xie, Y.; Kang, K.; Song, H.; Bai, S.; Han, H.; Li, S. Efficient Adsorption of Ammonia by Surface-Modified Activated Carbon Fiber Mesh. *Nanomaterials* **2023**, *13* (21), 2857.
(25) International Union of Pure and Applied Chemistry (IUPAC) *Molecular Sieve Effect: IUPAC Compendium of Chemical Terminology (Gold Book)*; IUPAC, 2025. DOI: .
(26) Kretzschmar, A.; Selmert, V.; Weinrich, H.; Kungl, H.; Tempel, H.; Eichel, R. Tailored Gas Adsorption Properties of Electrospun Carbon Nanofibers for Gas Separation and Storage. *ChemSusChem* **2020**, *13* (12), 3180−3191.
(27) Selmert, V.; Kretzschmar, A.; Weinrich, H.; Tempel, H.; Kungl, H.; Eichel, R. CO_2/N_2 Separation on Highly Selective Carbon Nanofibers Investigated by Dynamic Gas Adsorption. *ChemSusChem* **2022**, *15* (14), No. e202200761.
(28) Selmert, V.; Kretzschmar, A.; Kungl, H.; Tempel, H.; Eichel, R.-A. Breakthrough Analysis of the CO_2/CH_4 Separation on Electrospun Carbon Nanofibers. *Adsorption* **2024**, *30* (1), 107−119.
(29) Kretzschmar, A.; Selmert, V.; Kungl, H.; Tempel, H.; Eichel, R.-A. Application of a Tailorable Carbon Molecular Sieve to Evaluate Concepts for the Molecular Dimensions of Gases. *Microporous Mesoporous Mater.* **2022**, *343*, 112156.
(30) Ravikovitch, P. I.; Vishnyakov, A.; Russo, R.; Neimark, A. V. Unified Approach to Pore Size Characterization of Microporous Carbonaceous Materials from N_2, Ar, and CO_2 Adsorption Isotherms. *Langmuir* **2000**, *16* (5), 2311−2320.
(31) *Autosorb iQ/ASiQwin Operating Manual*; Quantachrome Instruments, 2015.
(32) Sips, R. On the Structure of a Catalyst Surface. *J. Chem. Phys.* **1948**, *16* (5), 490−495.
(33) Azizian, S.; Eris, S. Chapter 6 - Adsorption Isotherms and Kinetics. In *Interface Science and TechnologyAdsorption: Fundamental Processes and Applications*; Ghaedi, M., Ed.; Elsevier, 2021; Vol. 33, pp. 445−509. DOI: .
(34) Rouquerol, F.; Rouquerol, J.; Sing, K. *Adsorption by Powders and Porous Solids*; Elsevier, 1999. DOI: .
(35) Lagergren, S. Zur Theorie der sogenannten Adsorption gelöster Stoffe. *Zeitschr F Chem. Und Ind. der Kolloide* **1907**, *2* (1), 15.
(36) Azizian, S. Kinetic Models of Sorption: A Theoretical Analysis. *J. Colloid Interface Sci.* **2004**, *276* (1), 47−52.
(37) Cipriani, E.; Zanetti, M.; Bracco, P.; Brunella, V.; Luda, M. P.; Costa, L. Crosslinking and Carbonization Processes in PAN Films and Nanofibers. *Polym. Degrad. Stab.* **2016**, *123*, 178−188.
(38) Ye, L.; Lo, B. T. W.; Qu, J.; Wilkinson, I.; Hughes, T.; Murray, C. A.; Tang, C. C.; Tsang, S. C. E. Probing Atomic Positions of Adsorbed Ammonia Molecules in Zeolite. *Chem. Commun.* **2016**, *52* (16), 3422−3425.
(39) Wang, J.; Lou, F.; Zhang, M.; Yuan, J. Recent Progress in Nitrogen-Doped Activated Carbon: Microstructural Regulation and Enhanced Gas Adsorption. *J. Environ. Chem. Eng.* **2025**, *13* (5), 118107.
(40) Thommes, M.; Kaneko, K.; Neimark, A. V.; Olivier, J. P.; Rodriguez-Reinoso, F.; Rouquerol, J.; Sing, K. S. W. Physisorption of Gases, with Special Reference to the Evaluation of Surface Area and Pore Size Distribution (IUPAC Technical Report). *Pure Appl. Chem.* **2015**, *87* (9−10), 1051−1069.
(41) Schierholz, R.; Kröger, D.; Weinrich, H.; Gehring, M.; Tempel, H.; Kungl, H.; Mayer, J.; Eichel, R.-A. The Carbonization of Polyacrylonitrile-Derived Electrospun Carbon Nanofibers Studied by *in Situ* Transmission Electron Microscopy. *RSC Adv.* **2019**, *9* (11), 6267−6277.
(42) Park, J.; Kretzschmar, A.; Selmert, V.; Camara, O.; Kungl, H.; Tempel, H.; Basak, S.; Eichel, R. A. Structural Study of Polyacrylonitrile-Based Carbon Nanofibers for Understanding Gas Adsorption. *ACS Appl. Mater. Interfaces* **2021**, *13* (39), 46665−46670.
(43) Sircar, S.; Cao, D. V. Heat of Adsorption. *Chem. Eng. Technol.* **2002**, *25* (10), 945−948.
(44) Guo, X.; Wang, J. A General Kinetic Model for Adsorption: Theoretical Analysis and Modeling. *J. Mol. Liq.* **2019**, *288*, 111100.
(45) Pooresmaeil, M.; Namazi, H. Application of Polysaccharide-Based Hydrogels for Water Treatments. In *Hydrogels Based On Natural Polymers*; Elsevier, 2020, pp.411−455. DOI:
(46) Wang, J.; Guo, X. Adsorption Kinetic Models: Physical Meanings, Applications, and Solving Methods. *J. Hazard. Mater.* **2020**, *390*, 122156.
(47) Chen, F.; Shang, H.; Hai, G.; Huang, X.; Chu, Z.; Sun, H.; Yang, L.; Yang, Q.; Zhang, Z.; Ren, Q.; Bao, Z. Sub-Ångstrom Pore Engineering in Carbon Molecular Sieves Realizes Diffusion-Gated Kinetic Sieving of Alkenes from Alkanes. *Angew. Chem., Int. Ed.* **2025**, *64* (36), No. e202513448.
(48) Cardenas, C.; Sigot, L.; Vallières, C.; Marsteau, S.; Marchal, M.; Latifi, A. M. Ammonia Capture by Adsorption on Doped and Undoped Activated Carbon: Isotherm and Breakthrough Curve Measurements. *Sep. Purif. Technol.* **2023**, *313*, 123454.
(49) Hindocha, S.; Poulston, S. Study of the Scale-up, Formulation, Ageing and Ammonia Adsorption Capacity of MIL-100(Fe), Cu-BTC and CPO-27(Ni) for Use in Respiratory Protection Filters. *Faraday Discuss* **2017**, *201*, 113−125.